Contents lists available at ScienceDirect

Bioactive Materials

journal homepage: www.sciencedirect.com/journal/bioactive-materials

Antibiotic-loaded amphora-shaped pores on a titanium implant surface enhance osteointegration and prevent infections

Viviane Ständert [a,1], Kai Borcherding [b,1], Nicole Bormann [a], Gerhard Schmidmaier [c], Ingo Grunwald [d], Britt Wildemann [a,e,*]

[a] *Julius Wolff Institute, BIH Center for Regenerative Therapies, Charité, Universitätsmedizin Berlin, Corporate Member of Freie Universität Berlin, Humboldt-Universität zu Berlin, Berlin Institute of Health, 13353, Berlin, Germany*
[b] *Department of Adhesive Bonding Technology and Surfaces, Fraunhofer Institute for Manufacturing Technology and Advanced Materials (IFAM), 28359, Bremen, Germany*
[c] *Center for Orthopedics, Trauma Surgery and Spinal Cord Injury, HTRG - Heidelberg Trauma Research Group, Heidelberg University Hospital, 69118, Heidelberg, Germany*
[d] *Industrial and Environmental Biology, Hochschule Bremen-City University of Applied Sciences, 28199, Bremen, Germany*
[e] *Experimental Trauma Surgery, Department of Trauma, Hand and Reconstructive Surgery, Jena University Hospital, Friedrich Schiller University Jena, 07747, Jena, Germany*

ABSTRACT

Artificial prostheses for joint replacement are indispensable in orthopedic surgery. Unfortunately, the implanted surface is attractive to not only host cells but also bacteria. To enable better osteointegration, a mechanically stable porous structure was created on a titanium surface using laser treatment and metallic silver particles were embedded in a hydrophilic titanium oxide layer on top. The laser structuring resulted in unique amphora-shaped pores. Due to their hydrophilic surface conditions and capillary forces, the pores can be loaded preoperative with the antibiotic of choice/need, such as gentamicin. Cytotoxicity and differentiation assays with primary human osteoblast-like cells revealed no negative effect of the surface modification with or without gentamicin loading. An *in vivo* biocompatibility study showed significantly enhanced osteointegration as measured by push-out testing and histomorphometry 56 days after the implantation of the K-wires into rat femora. Using a *S. aureus* infection model, the porous, silver-coated K-wires slightly reduced the signs of bone destruction, while the wires were still colonized after 28 days. Loading the amphora-shaped pores with gentamicin significantly reduced the histopathological signs of bone destruction and no bacteria were detected on the wires. Taken together, this novel surface modification can be applied to new or established orthopedic implants. It enables preoperative loading with the antibiotic of choice/need without further equipment or post-coating, and supports osteointegration without a negative effect of the released dug, such as gentamicin.

1. Introduction

Total joint arthroplasty (TJA) is primarily performed on older patients suffering from the degenerative destruction of the joint or osteoporotic fracture. In light of demographic trends, an increase in TJAs is expected [1]. To improve the integration of the prosthesis and thereby optimize its lifetime, surface modifications, e.g. based on hydroxyapatite, have been developed and successfully used for decades [2]. Periprosthetic joint infection (PJI), however, is still a severe complication of TJA and is associated with increased morbidity risk [3]. Despite an increased awareness of the PJI risk and new prevention strategies, surgical site infections following hip and knee arthroplasty are expected to increase by 14% over the next 10 years [4]. Therefore, further strategies are needed to reduce the growing burden of PJI [3].

One cause of PJI is implant-associated infection (IAI). Whenever a material is implanted into the body, it evokes a local immune response, which impairs the bacterial clearance [5,6]. The bacteria and host cells then start to colonize the material surface. Depending on the winner of the "race for the surface" [7], either an IAI develops or the implant becomes integrated into the host bone. Various approaches have been developed to direct the race for the surface towards osteoblast adherence and, hence, osteointegration. The antibacterial properties of an implant surface are based on passive or active surface modification (PSM or ASM) [8]. PSM inhibits bacterial adherence due to a modified surface chemistry or surface topography [9]. In general, hydrophilic surface conditions [10], structured surface topography [11] and porous structures [12] can enhance the osteointegration of the implant. Laser surface treatments for improved osteointegration are the state of the art, but these differ in terms of the details of the respective surface topographies. The coalescence between bone and the implant can be promoted by a nanostructured laser surface, as shown *in vivo* [13]. Surface modifications such as pore size, porosity, and structure highly affect the interaction of the implant with the surrounding tissue and influence osteointegration and vascularization, as summarized in a review for additively manufactured titanium implants [14].

ASM is designed to locally release anti-infective substances and eradicate bacteria without being in direct contact with the implant. Various strategies for the loading of surfaces with antimicrobial substances have been studied and are summarized in reviews [15,16]. From a translational point of view, the surface modification should be applicable for well-established implants, allow the loading with the necessary antimicrobial drug, and be performed intraoperatively within the appropriate time. To address these points, this study used laser-structuring technology. We already showed that the produced surface combines pores of the suggested size for bone ingrowth with undercuts for interlocking and the cell-attractive surface of titanium dioxide [17]. The amphora-shaped pores of the laser-structured surface can be loaded with antibiotics such as gentamicin without further equipment or post-coating, and the initial burst release will eradicate the bacteria contaminating the wound/bone or implant. The silver coating should provide a protective effect over a longer period when bacteria might come in contact with the implant via the systemic path; therefore, a slow and low release is realized [18]. The current study aims to investigate 1) the cytocompatibility *in vitro* and biocompatibility *in vivo* of the surface modification with and without gentamicin loading and 2) the antimicrobial effect against *Staphylococcus aureus* and infection prevention in a rat infection model.

2. Material and methods

2.1. Test specimen and surface characterization

2.1.1. Structural and adhesion/cohesion characterization

Titanium grade 5 plates (ARA-T Advance GmbH, Dinslaken, Germany) were treated with a Q-switched Nd:YAG laser ($\lambda = 1064$ nm) type CL100 with an average power of 100 W (Clean Lasersysteme GmbH, Herzogenrath, Germany) to create amphora-shaped pores 70–160 μm in length and 40–70 μm in width in the titanium surface. A high-frequency sputtering chamber (Fraunhofer IFAM, Bremen, Germany) was then used to embed silver-nanoparticles (10–30 nm) in a porous titanium-dioxide coating (4 μg/cm^2) on top of the structure by magnetron sputtering. For a more detailed description of the surface modification and applied characterization methods, see recent publications [17,18]. The adhesion/cohesion of the generated structure (Porous) was evaluated against the control (CTRL) using the following tests: in regard to horizontal force, a lap-shear test (based on DIN EN 1465:2009–07), in regard to vertical force, a pull-off test (based on DIN EN ISO 4624:2016–08), and in regard to impact force, a scratch test (based on DIN 55656:2014–12). In addition, to evaluate cohesion under bending, a four-point bending test (based on ASTM F1264 - 16e1) was also performed.

The plates for the lap shear tests had the dimensions 100.5 mm length x 24.8 mm width x 3.0 mm height. For the Porous samples, an area of 23.5 mm x 24.8 mm at one end of each plate was laser structured. A single overlap joint of 12.5 mm was performed with a two-component epoxy adhesive (Araldite® 2011, Huntsman Advanced Materials, Basel, Switzerland). This epoxy adhesive is capable of achieving lap shear strengths of metal-to-metal joints in the range of 22–26 MPa [19]. For the pull-off tests, plates (51 mm x 51 mm x 3 mm) in combination with sand-blasted test dollies (20 mm diameter) were bonded with the same epoxy adhesive. For the Porous pull-off samples, an area of 35 mm x 35 mm in the middle of the plates was laser structured. Both tests were performed using an A Z020 testing machine (Zwick Roell GmbH & Co. KG, Ulm, Germany). The results were reported as measured force at rupture, and the stressed surfaces were inspected regarding adhesive and cohesive failure modes. The influence of an impact force on the laser-structured area was evaluated by a scratch tester with a 1.0 mm needle (DUR-O-Test, BYK-Gardner GmbH, Geretsried, Germany) on titanium plates (20 mm x 20 mm x 1 mm). A force up to 20 N was applied. The introduced scratches were compared in size and inspected regarding cohesive failure. The surfaces were captured by a VHX-1000 digital microscope with a VH-Z 100 lens (Keyence Int. Trading Co. Ltd., Osaka, Japan) and further profilometric assessments of the scratches were performed using a PLu neox optical profiler (SENSOFAR TECH, Barcelona, Spain). Complementary to the impact force evaluation, a further possibility for the delamination of the laser-structured area under load was determined by four-point bending tests. The tests were conducted in a Z100 testing machine (Zwick Roell GmbH & Co. KG, Ulm, Germany). The span was 120 mm and the inner loading points had a distance of 40 mm. Titanium rods (160 mm length x 10 mm diameter) were tested (TORLOPP Industrie-und Messtechnik GmbH, Dägeling, Germany). For porous samples, an area 55 mm in length in the middle of the rod was laser structured. The bending modulus was determined, and the surfaces were inspected regarding cohesive failure in the area of bending.

2.1.2. Surface wettability

Dynamic contact angle (wettability) measurements of the K-wires (mahe medical GmbH, Emmingen-Liptingen, Germany) were performed according to the Wilhelmy method [20] using a DCAT 11 tensiometer (DataPhysics Instruments GmbH, Filderstadt, Germany) in combination with a CHROMASOLV Plus water (Honeywell Specialty Chemicals Seelze GmbH, Seelze, Germany). The advancing and receding contact angles were calculated using SCAT software version 2.8.1.77 (Data-Physics Instruments GmbH, Filderstadt, Germany).

2.1.3. Test specimen

The laser structuring process increased the dimension of the samples due to the generated porosity: the diameter of the 1.0 mm titanium K-wires increased by 0.1 mm. This was taken into consideration in the animal studies and adapted accordingly. The following K-wire diameters were used: a) cyto- and biocompatibility study median CTRL and median Porous: 1.4 mm; and b) infection study median CTRL and median Porous: 1.1 mm. Gentamicin loading took place directly before implantation/incubation. The K-wires were immersed in a 250 mg/mL gentamicin sulfate solution (Carl Roth GmbH + Co. KG, Karlsruhe, Germany) for 5 min, pulled through a polytetrafluoroethylene-faced butyl septum (Merck KGaA, Darmstadt, Germany) to remove excessive fluid, and air-dried for 3–5 min. Due to the different diameters of the K-wires for the osteointegration and infection studies, gentamicin loadings of 395 ± 15 μg/cm^2 for the 1.1 mm and 435 ± 10 μg/cm^2 for the 1.4 mm wires were obtained. Fig. 1 shows the surface modification and the implants used for the studies.
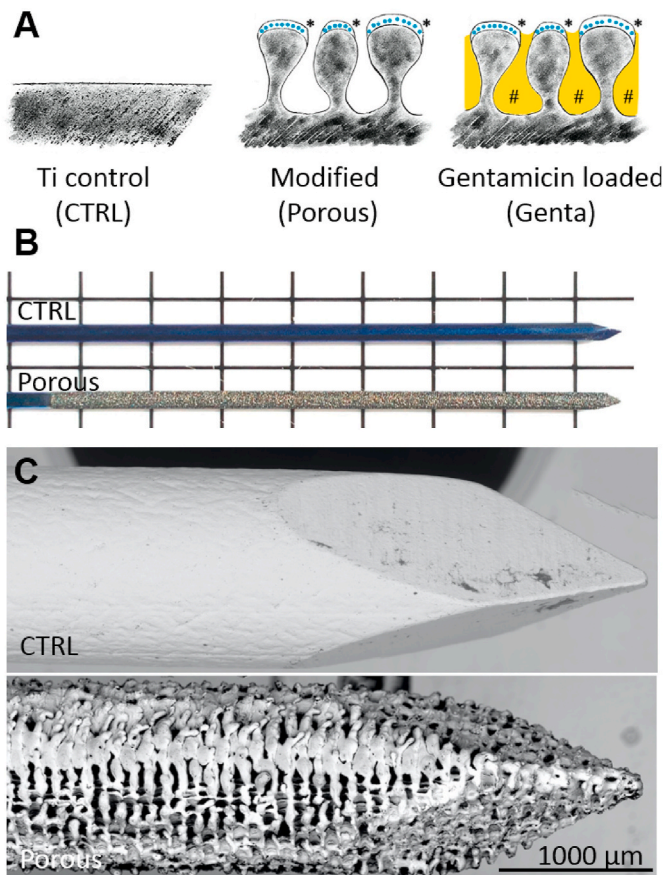
Fig. 1. Schematic drawing and pictures of the surface modification. A) The three investigated surfaces were smooth titanium (CTRL), the modification of the titanium surface with the amphora-shaped pores and the silver deposition (* blue dots) in the titanium oxide layer (Porous), and the porous surface loaded with gentamicin (# yellow) (Genta). B) The macroscopic changes of the wire due to the laser treatment. C) The tips of the K-wires without and with laser treatment; the porous structure of the modified surface is clearly visible.

2.2. Cyto- and biocompatibility study

2.2.1. Cells and groups

Primary human osteoblast-like cells from four donors (2 males and 2 females, aged 60–85 years, cells isolated from the femoral head, IRB approval: EA4/035/14) in passage 2 were pooled. The patients gave written informed consent. Cells were cultured in DMEM/Ham's F-12 medium (Biochrom, Berlin, Germany) with 10% fetal bovine serum (FBS; Biochrom, Berlin, Germany), 1% penicillin/streptomycin (P/S; Biochrom, Berlin, Germany) and freshly supplemented 0.05 mM L-ascorbic acid (L-Asc) and 0.05 mM β-glycerol phosphate (β-Gly) (both Sigma-Aldrich/Merck, Darmstadt, Germany), henceforth called growth medium (GM).

The following groups were analyzed: 1) cells only (Medium), 2) titanium K-wire (CTRL), 3) porous K-wire (Porous), and 4) porous K-wire loaded with gentamicin (Genta). The porous K-wires of group 3 and 4 were coated with silver nanoparticles. For the cytocompatibility test, a toxic control was used: 5) 10% 2-hydroxyethyl methacrylate (HEMA; Positive). The experiments were done in triplicate and repeated once, resulting in n = 6 per group. For the experiments, 1.4 mm K-wire pieces (7 mm length) were transferred to inserts (10 mm diameter and polycarbonate membrane with 8 μm pores; Thermo Scientific/Nunc, Schwerte, Germany) and placed in the culture wells.

2.2.2. Cytocompatibility

Cells $(3*10^4)$ were cultured in 24-well plates under standard conditions (5% CO_2, 95% humidity at 37 °C). After overnight incubation, the medium was removed and metabolic cell activity was measured with PrestoBlue® (Invitrogen, Karlsbad, CA, USA) in triplicate according to the manufacturer's instructions. Afterwards, the cells were starved in the medium with only 0.1% FBS and without P/S and supplements (starving medium) for 1 h and the transwells with the K-wires were added.

After three days of cultivation, the PrestoBlue assay was followed by an alkaline phosphatase (AP) activity assay using 0.13% w/v 4-nitrophenyl phosphate disodium salt hexahydrate (p-NPP, Sigma-Aldrich/Merck, Darmstadt, Germany) dissolved in 0.1 M AP-buffer pH 10.5 (50 mM glycine, 100 mM Tris-Base, 1 mM $MgCl_2$ in dH_2O). Cells were incubated for 30 min at 37 °C and absorbance was read in triplicate at a wavelength of 405 nm.

2.2.3. Differentiation

Cells $(3*10^4)$ were seeded in 24-well plates and cultivated under standard conditions to a minimum confluence of 80% (about 5–7 days). At day 0, the PrestoBlue assay was done as described above. The cells were then cultured in growth medium (GM) or in osteogenic differentiation medium (DM: DMEM/Ham's F-12 medium with 10% FCS and freshly added 0.5 mM L-Asc, 10 mM β-Gly, 1.5 mM calcium chloride, 10 nM dexamethasone) with a complete medium change every 3–4 days. After 21 days, the following assays were performed: PrestoBlue assay, AP activity assay, and Alizarin red quantification.

Matrix mineralization was evaluated using Alizarin red staining. Cells were fixed with 4% PFA for 10 min at room temperature (RT) and incubated with 0.5% w/v Alizarin red (Sigma-Aldrich/Merck, Darmstadt, Germany) in dH_2O for 10 min at RT. For quantification, cells were rinsed with 5% w/v sodium dodecyl sulfate (SDS; Sigma-Aldrich/Merck, Darmstadt, Germany) in 5 mM HCl and the absorbance was measured at 405 nm.

The PrestoBlue data at the end of the experiment were normalized to the data from day 0, while the AP activity and Alizarin red quantification were normalized to the PrestoBlue data from the same day. The data are shown as the fold change to the CRTL group (titanium).

2.2.4. Biocompatibility in vivo

2.2.4.1. Animals and surgical procedure.
A total of 48 five-month-old female Sprague Dawley rats (Janvier Labs, Le Genest-Saint-Isle, France) with a mean bodyweight of 311 ± 12 g were used in this study. The experiments were approved by the Animal Experimentation Ethics Committee of Berlin (project number G0072/18), complied with the ARRIVE guidelines, and were carried out in accordance with the EU Directive 2010.

The rats were housed in conventional Type IV cages with a 12-h day and night cycle in groups of four. They were fed a standard rodent chow (ssnif Spezialdiäten GmbH, Soest, Germany) and water ad libitum. After arriving at the animal facility, the animals were acclimated for a period of at least 7 days. The rats were randomly divided into three groups with 16 rats per group, resulting in 8 rats for mechanical testing and 8 rats for histology per group: 1) titanium K-wire (Control, CTRL), 2) porous K-wire (Porous), and 3) porous K-wire with 435 μg/cm^2 gentamicin (Genta). The porous K-wires of group 2 and 3 were coated with silver nanoparticles.

The surgical procedures took place under inhalation anesthesia with isoflurane (Abbott GmbH & Co. KG, Wiesbaden, Germany). Preoperatively, each rat was administered 0.04 mg/kg buprenorphine (Temgesic®, Indivor UK Limited, Berkshire, United Kingdom) subcutaneously for analgesia. The fur on the right hind leg was clipped and disinfected with a povidone-iodine solution (Braunoderm®, B. Braun, Melsungen, Germany). Eye ointment was applied (Bepanthen® Augensalbe, Bayer AG, Leverkusen, Germany) and the rats were placed on a heating mat during the entire procedure. Under sterile conditions, a small

parapatellar incision (0.5 cm) was performed and the patella was dislocated laterally to expose the femoral condyles. A hole in the intercondylar fossa was drilled manually with a 1.2 mm K-wire and reamed until 2 mm width. Afterwards, a 1.4 mm K-wire (material according to the group) was inserted and cut as close as possible to the femoral surface with a side cutter. The cortical defect was sealed with bone wax (Ethicon, Bridgewater, USA) and the wound was closed layer by layer with the single knot technique (Vicryl 3-0 absorbable, Ethicon 3-0 non-absorbable, Ethicon, Bridgewater, US).

2.2.4.2. Follow-up. All animals received postoperative oral analgesia with tramadol 0.5 mg/mL (Tramal, Grünenthal GmbH, Aachen, Germany) for five days.

In the first five days following the operation, the animals were checked daily, and afterwards 2–3 times weekly, concerning their weight, general behavior, gait and wound healing. On day 0, 7, 28 and 56, radiographs were taken under inhalation anesthesia.

After 56 days the rats were sacrificed by final cardiac puncture after an intraperitoneal injection of 60 mg/kg ketamine (ketamine 10%, cp pharma, Burgdorf, Germany) and 0.3 mg/kg medetomidine (Cepetor, cp pharma, Burgdorf, Germany).

2.2.4.3. Radiography. The position of the K-wire was checked by x-ray immediately after surgery and during the follow-up. An osteointegration score modified from Das et al. [11] was used to evaluate the macroscopic and radiographic changes in soft tissue swelling, implant movement, surface irregularities, hyperplastic growth/periosteal reactions, and peri-implant bone radiolucency. Each parameter was scored from 0 (no changes) to 3 (severe changes). To obtain an additive score, the values were summed up with a maximum of 15 points.

2.2.4.4. Biomechanical testing. To investigate the osteointegration of the K-wires into the femora, push-out tests were performed. The femora were explanted and all soft tissue was removed. At the distal end of the trochanter minor and proximal of the facies poplitea, a circular incision was made using a small disc saw to expose the pin ends. The lengths of the remaining bone were measured with a digital caliper (IP67, TESA Hexagon, Stockholm, Sweden). To ensure sufficient stability during the test, the distal part of the femur was embedded with Technovit 3040 (Kulzer Technik, Hanau, Germany) in a standardized manner. It was ensured that the embedding medium had no contact with the exposed pins. The push-out was performed at a speed of 2 mm/min. The push-out tests on the first operated rats were done with a Bose Test Bench LM 1 ElectroForce (Bose, Eden Prairie, MN, USA). The K-wires were loaded at a rate of 2 mm/min and the force was measured with a 225 N load cell. Displacement and force data were sampled at 100 Hz. The maximum force reached higher values than expected and were at the upper limit of the system. Therefore, a Z010 testing machine (Zwick/Roell, Ulm, Germany) with a 10 kN load cell that allowed the application of higher forces was used instead. The same load rate and data sample frequency were used. The push-out force needed was in a comparable range independent of the used system (Bose vs. Zwick). After measuring the maximal push-out forces, the shear stress (MPa) was calculated to compensate for the different femur lengths [21].

2.2.4.5. Histomorphometric analysis. The femora were explanted and, after careful removal of the soft tissue, fixed with 4% buffered formaldehyde-solution (SAV Liquid Production GmbH, Flintsbach am Inn, Germany) for three days at room temperature. After dehydration in ascending concentrations of ethanol, the femora were infiltrated and embedded in Technovit 7200 (Kulzer Technik, Hanau, Germany). A band saw (EXAKT 300, EXAKT, Norderstedt, Germany) was used to trim the samples to 500 μm thickness. Cutting directly through the pin was avoided due to the possible loosening of the K-wire. Afterwards, the samples were ground to 80 μm using an EXAKT 400CS grinding machine

(EXAKT, Norderstedt, Germany) and stained with van Kossa/Safranin orange staining. Microscopical digital images were taken (Axioskop40, Zeiss, Oberkochen, Germany). A line determining the region of interest (ROI, approximately 13.7 mm, proximal diaphysis, [21]) was drawn (ImageJ, U. S. National Institutes of Health, Bethesda, Maryland, USA, [22]). Only the diaphyseal areas were analyzed because the irregular spongy bone structure of the epiphyseal region interfered with the analysis in that newly formed bone is harder to distinguish from old bone in that area. This allowed a better comparison with the push-out analysis, where the condyles were removed during preparation. The bone-implant contact (BIC) was calculated. Furthermore, the length of connective tissue that formed around the entire K-wires was measured and compared to the total length of the K-wire. Each sample was measured three times and the mean was used for the statistical analysis.

2.3. Antibacterial activity

2.3.1. Bacteria

S. aureus (ATC 25923, German Collection of Microorganisms and Cell Cultures GmbH, Braunschweig, Germany) cultures were freshly prepared for each experiment. Hereby, one cryoconserved Mikrobank bead was rolled over Columbia Agar (CA) with sheep blood (Oxoid, Wesel, Germany) and incubated for 24 h at 37 °C. Single colonies were dissolved in PBS, and the required concentration of CFU/mL was achieved using a McFarland standard protocol (Densimat, bioMérieux, Marcy l'Etoile, France).

2.3.2. Release experiment

Coated and uncoated K-wires were cut into pieces of 7 mm each, placed in 2 mL tubes (Eppendorf, Hamburg, Germany) pre-filled with 1 mL phosphate-buffered saline (PBS; Gibco/Thermo Fischer Scientific, Waltham, USA), and incubated at 37 °C for 3 days. At time points 30 min, 1 h, 4 h, 1 day and 3 days, 500 μL samples were taken and refilled with 500 μL fresh PBS. Elution samples and wires were stored at −20 °C.

Gentamicin was quantified by Labor Berlin-Charité Vivantes GmbH (Berlin, Germany) using the method known as the 'kinetic interaction of microparticles in a solution' (KIMS; Roche Diagnostics, Mannheim, Germany). The cumulative release was calculated [23].

2.3.3. Zone of inhibition test (ZOI)

A McFarland 1 was produced from *S. aureus* colonies (see the section on bacteria). The bacteria solution was diluted 1:1 with PBS and plated on Müller-Hinton plates (Oxoid, Wesel, Germany) with cotton swabs. Filter discs (Ø 6 mm, Oxoid, Wesel, Germany) were placed on the plates and elution samples (15 μL) from all time points were pipetted onto each filter. Additionally, wires from the elution experiment (3 days elution) and wires without elution were added to the plates. The plates were incubated overnight at 37 °C and photographed the next day. Zones of inhibition were determined using ImageJ software (Version 1.41.o, National Institute of Health, Maryland, USA).

2.3.4. Infection model

2.3.4.1. Animals and surgical procedure. In total, 32 female 8 ± 2 month old Sprague Dawley rats (Janvier Labs, Le Genest-Saint-Isle, France) with a mean bodyweight of 391 ± 51 g were housed in standard Type IV cages in groups of four pre-operatively, and in groups of two after the procedure. For the husbandry circumstances and animal experimental approval, see 2.2.4.1.

The following groups with n = 8 were investigated:

1) Titanium K-wire (Control, CTRL): inoculation with 50 μL PBS, implantation of unmodified K-wire; 2) Infection: inoculation with 50 μL *S. aureus*, implantation of unmodified K-wire; 3) Porous: inoculation with 50 μL *S. aureus*, implantation of porous silver-coated K-wire; 4) Genta: inoculation with 50 μL *S. aureus*, implantation of porous silver-

coated K-wire loaded with 395 μg/cm^2 gentamicin.

All K-wires had a diameter of 1.1 mm.

The animals of the control group received inhalation anesthesia with isoflurane (Abbott GmbH & Co. KG, Wiesbaden, Germany). The isoflurane anesthesia caused bleeding from the intramedullary canal, causing problems with the bacteria inoculation. Therefore, the animals from the infection group were anaesthetized by an intraperitoneal injection of 60 mg/kg ketamine (ketamine 10%, cp pharma, Burgdorf, Germany) and 0.3 mg/kg medetomidine (Cepetor, cp pharma, Burgdorf, Germany) and prepared for surgery as described in 2.2.4.1.

The intramedullary canal was reamed until a 1.2 mm width and blood was aspirated from the bone marrow canal. Then, 50 μL of the bacterial solution ($5*10^6$ CFU) was inoculated with a 1 mL syringe and a G24 needle. The K-wire (surface modification according to the group) was implanted directly afterwards and shortened as close as possible to the femoral surface with a side cutter. The implant site was sealed with bone cement (Bosworth Trim, Kystone Industries, New Jersey, USA). The surrounding soft tissue was disinfected with Braunol® (B. Braun, Melsungen, Germany) and the wound was closed layer by layer (Vicryl 3-0 absorbable, Ethicon 3-0 non-absorbable, Ethicon, Bridgewater, USA). Anesthesia was reversed with 0.75 mg/kg atipamezole (Revertor, cp pharma, Burgdorf, Germany). For analgesia, 0.04 mg/kg buprenorphine was administered subcutaneously (Temgesic®, Indivor UK Limited, Berkshire, United Kingdom). The animals were checked twice a day in the first 5 days after the surgery regarding their weight, general behavior, gait, and wound healing. During this period, they received oral analgesia with tramadol via their water at 0.5 mg/mL (Tramal, Grünenthal GmbH, Aachen, Germany). Afterwards, check-ups were carried out 2 to 3 times a week.

The rats were euthanized on the 28th postoperative day with a peritoneal injection of 60 mg/kg ketamine and 0.3 mg/kg medetomidine followed by a final cardiac puncture.

The K-wires were explanted and rolled over CA. Then, they were placed in 2 mL tubes with PBS (Eppendorf AG, Hamburg, Germany), sonicated for 1 min at 800 W/40 kHz (BactoSonic, BANDELIN electronic GmbH & Co. KG, Berlin, Germany), and plated on CA (with and without dilution). All agar plates were incubated at 37 °C for 24 h. The colonies were counted, Gram stained with a commercial kit (Carl Roth GmbH & Co. KG, Karlsruhe, Germany), and evaluated microscopically.

2.3.4.2. Radiology and histology. The K-wires were explanted, the hind legs were amputated, and radiographs were taken. The bones were scored using an adapted score [24] to evaluate the periosteal reaction, radiolucency, and surface irregularity on the femoral condyles, ranging from 0 (no changes) to 3 (severe changes); the result was a maximum score of 9. Afterwards, the femora were dissected from all soft tissue and fixed with 4% buffered formaldehyde solution for 3 days at room temperature. The samples were decalcified with an EDTA-based decalcifier (Solvagreen®, Carl Roth GmbH + Co. KG, Karlsruhe, Germany) for 21–28 days at 37 °C, dehydrated automatically for 3 days (Leica TP 1020, Leica Biosystems, Wetzlar, Germany), embedded in paraffin, and cut into 4–5 μm thick sections. Bacterial infection was confirmed with Gram staining (adapted protocol for paraffin sections, Gram staining kit, Carl Roth GmbH & Co. KG, Karlsruhe, Germany). To evaluate the degree of inflammation and to differentiate between acute, chronic, and chronically florid and subsided osteomyelitis, the Histopathological Osteomyelitis Evaluation Score (HOES) was used on HE stained sections [25]. The five categories of inflammatory patterns, which are divided into signs of acute osteomyelitis (like osteo- or soft tissue necrosis and granulocyte infiltration) and signs of chronic osteomyelitis (like bone neogenesis, fibrosis, lymphocyte and macrophage infiltration), were evaluated semi-quantitatively ranging from 0 (no signs) to 3 (severe signs) with a maximum score of 15. A score of ≥4 in the acute category is considered as signs of acute osteomyelitis, a score of ≥4 in the chronic category is considered as signs of chronic osteomyelitis and a score of ≤4 is considered as signs of subsided osteomyelitis. If the sum of all categories results in a score ≥6, it is interpreted as chronically fluid osteomyelitis. Microscopical digital photographs were taken with an Axioskop40 (Zeiss, Oberkochen, Germany).

2.4. Statistics

For the statistical analysis of two groups, the Mann-Whitney *U* test was used, and the multiple group comparison was performed with the Kruskal-Wallis test followed by Dunn's test (GraphPad Prism 8, San Diego, CA, USA). The *in vitro* cytotoxicity results were compared to the cytotoxic positive-group and the differentiation results were compared to the titanium control (CTRL). The data from the *in vivo* studies were compared between all groups. Values p ≤ 0.05 were considered as significant. The graphs and values in the text present the median values and the 25% and 75% quartiles.

3. Results

3.1. Surface modification

The cohesion of the porous surface with the implant is important and was analyzed with different methods. The surface response to the mechanical load was tested concerning a horizontal force (lap shear test) (Fig. 2A and B). The maximum tensile lap shear strength was significantly higher (p = 0.0079) for Porous samples (median: 26.31 MPa) compared to CTRL (median: 21.54 MPa). A non-significant difference was evaluated in the pull-off tests (p = 0.0952) for the Porous samples (median: 6.76 MPa) compared to CTRL (median: 3.74 MPa) (Fig. 2C and D). In the lap shear test, all Porous samples showed a cohesive failure mode within the adhesive, while the CTRL samples showed a failure mode of the adhesive from the surface. In the pull-off tests, three of the Porous samples showed a complete adhesive failure mode of the adhesive on the dolly surface. Two Porous samples showed a mixed failure type, with mainly adhesive failure on the dolly surface combined with slight (<25%) cohesive failure within the adhesive. One CTRL sample showed complete adhesive failure. The further four CTRL samples had cohesive failure within the adhesive combined with adhesive failure of the adhesive on the dolly surface. The following results were determined for cohesion under bending: A bending modulus of 92.03 ± 0.57 GPa for the Porous samples and 97.87 ± 3.65 GPa for CTRL. No peeling of the porous structure was observed after bending (Fig. 2E and F).

The impact force of 20 N (1 mm needle) applied with the scratch tester deformed the surfaces. A scratch with a 125 ± 10 μm width was observed for CTRL and 164 ± 22 μm for Porous samples (n = 3). The displacement, or rather deformation, of the metallic structure was visible in the profilometric measurements, but no peeling of the porous structure was observed (Fig. 2G–I).

Wettability, as an important surface characteristic for osteointegration, was assessed by dynamic contact angle measurements. The following contact angles were determined: 71 ± 6° advancing and 21 ± 5° receding measurement for the unmodified K-Wire (CTRL) and 9 ± 8° advancing and 9 ± 8° receding measurement for the modified K-wire (Porous), n = 3.

3.2. Cyto- and biocompatibility

3.2.1. Cytocompatibility

The effect of the structured K-wires with and without gentamicin on the metabolic activity and alkaline phosphate activity of human osteoblast-like cells was determined after three days. The cytotoxic control substance (HEMA) killed the cells and decreased the AP activity, while no negative effects due to the surface modification or gentamicin loading were observed (Fig. 3).

To test the effect of the structured K-wire and the gentamicin on the differentiation of osteoblast-like cells, the cells were cultured for 21 days
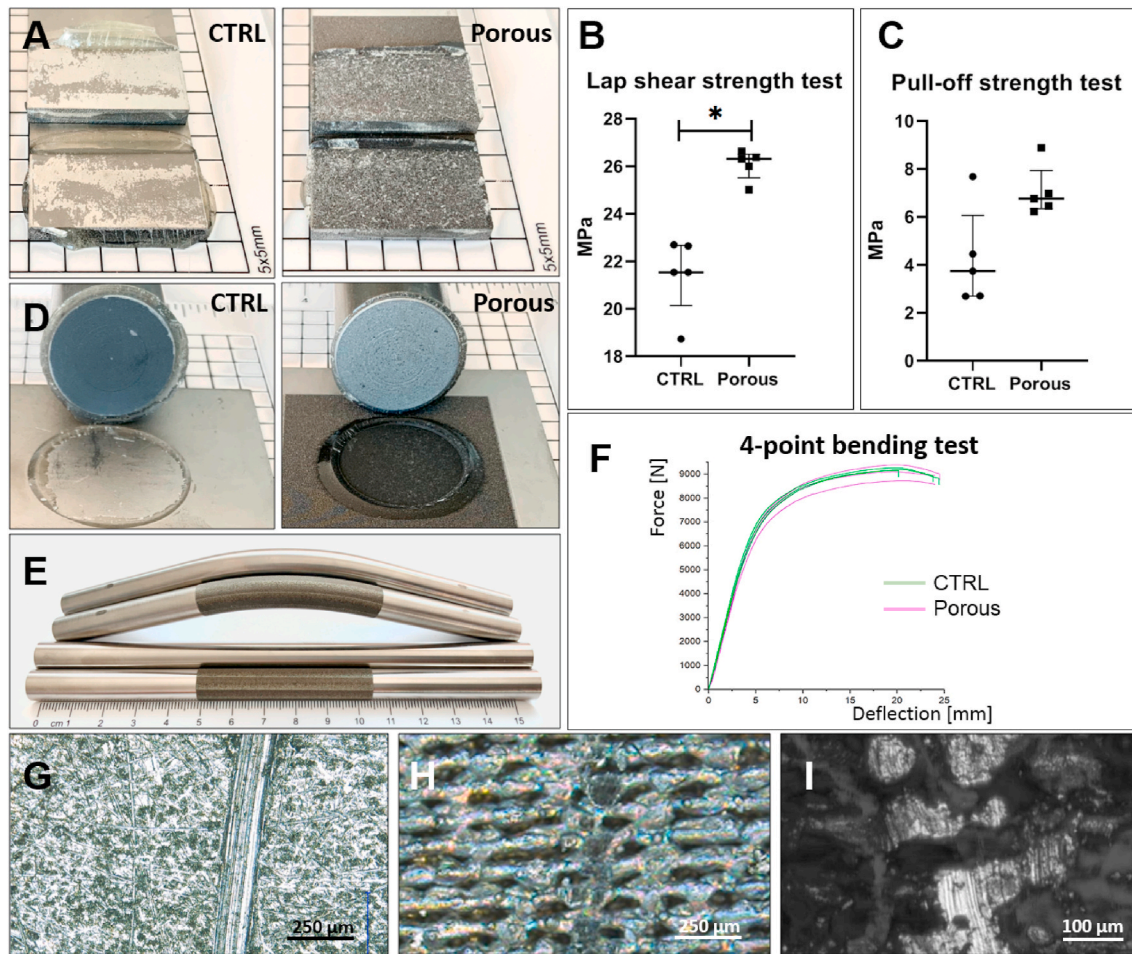
Fig. 2. The surface response to mechanical load. A) No cohesive failure of the porous structure was observed in the lap shear tests. B) The laser-structured surfaces (Porous) showed significant higher lap shear strengths; p = 0.0079 (n = 5). D) A comparable performance was achieved in the pull-off tests of the surfaces without and with structuring. C) The difference in pull-off strength was not significant (n = 5). E) The cohesion under bending was tested by 4-point bending and no peeling was observed after bending. F) Comparable forces were detected (n = 3). G - I) Instead of surface peeling, an impact force of 20 N resulted in a deformation of the surface. The scratch pattern on the Porous structure (H, I) was comparable to the CTRL surface (G) (representative pictures; total n = 3).
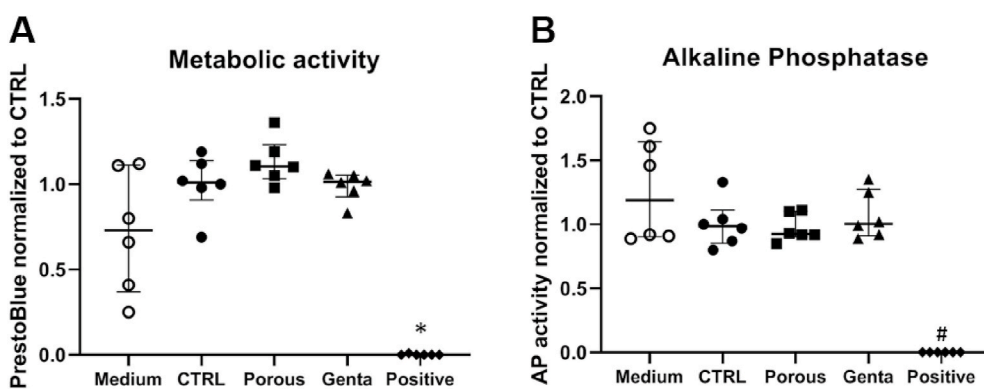

Fig. 3. Cytocompatibility assays with primary human osteoblast-like cells. Cells were cultured for three days with the medium only (Medium), the titanium control (CTRL), the modified K-wire (Porous), the gentamicin-loaded K-wires (Genta), and the toxic control (Positive); n = 6 samples per group. The positive/toxic-group showed a significant reduction in metabolic activity (A) (*p ≤ 0.0280 compared to CTRL, Porous, Genta) and alkaline phosphatase activity (B) (#p ≤ 0.0335 compared to Medium, CTRL, Porous, Genta). Statistics: all groups compared to the positive control; n = 6.

with growth medium (GM) or osteogenic differentiation medium (DM) (Fig. 4), and the metabolic activity, alkaline phosphatase activity, and mineralization (Alizarin red) were determined. The analyzed parameters were not negatively affected by the different K-wires or the gentamicin. When culturing the cells in the DM, alkaline phosphatase activity was significantly reduced by the gentamicin-loaded K-wires (p = 0.0453 compared to CTRL). Metabolic activity and mineralization were not affected.

3.2.2. Biocompatibility and osteointegration

One animal in the CTRL group showed a misplaced K-wire in the postoperative radiograph, resulting in immediate euthanasia. The animal was not replaced. The radiographic follow-up revealed no signs of osteolysis in any of the femora. Weight loss after the operation was minimal (0.3 ± 5 g) and all animals continued to gain weight until the end of the experiment, without differences between the groups. Five animals partially opened the sutures in the first days after the operation,
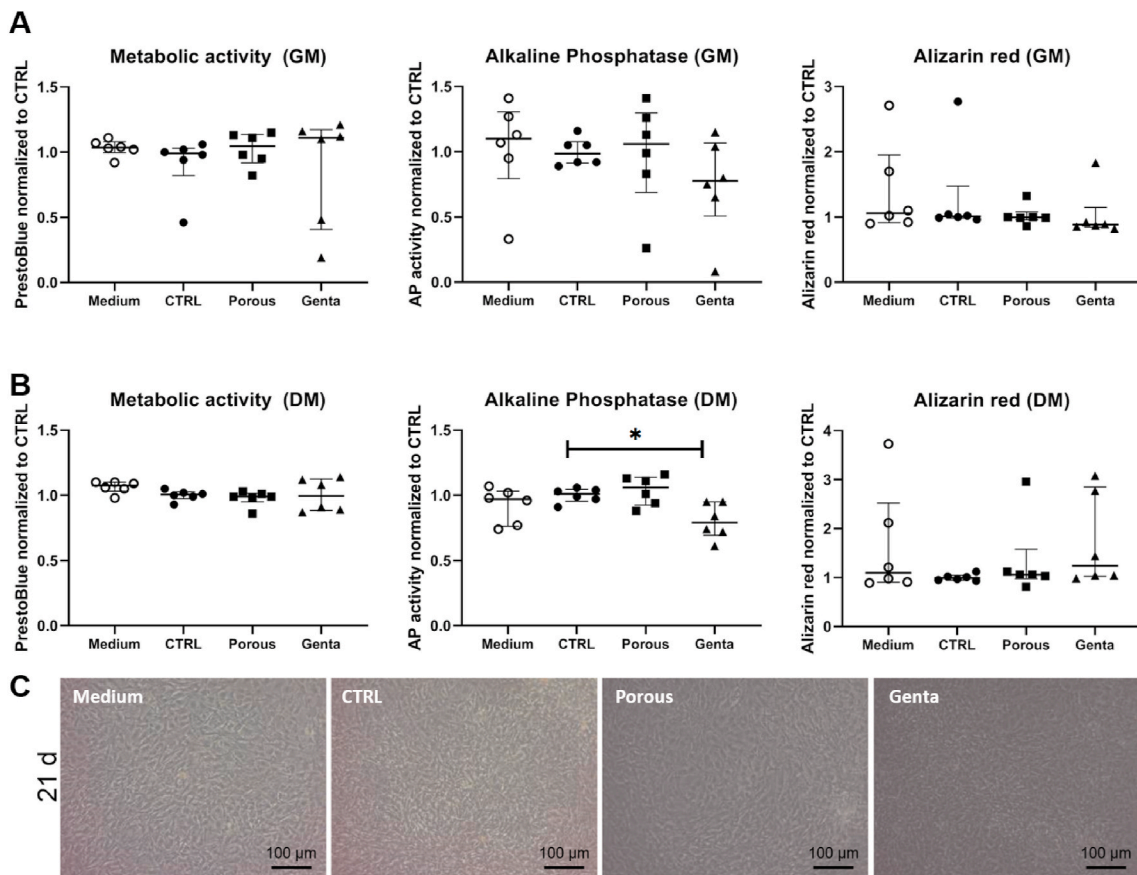
Fig. 4. Differentiation assay with primary human osteoblast-like cells. Cells were cultured for 21 days with medium only (Medium), the titanium control (CTRL), the modified K-wire (Porous), and the gentamicin-loaded K-wires (Genta) in growth medium (GM) or osteogenic differentiation medium (DM); n = 6 samples per group. A) GM: Culturing the cells with the different K-wires had no effect on the metabolic activity, the alkaline phosphatase activity or the mineralization (Alizarin red). B) DM: The gentamicin-loaded K-wires significantly reduced the alkaline phosphatase activity (p = 0.0453), while the other assays showed no significant alterations. Statistics: all groups compared to CTRL; n = 6. C) Exemplary pictures showing the cell morphology at day 21 in differentiation medium. No morphological differences were detectable between the groups.

resulting in partially secondary wound healing without signs of inflammation.

3.2.2.1. Radiology and biomechanical testing. Due to technical difficulties, no images were acquired from nine of the rats on day 7.

Consequently, day 7 was not included in the analysis. In general, the osteointegration score showed only small signs of structural alterations due to the implanted K-wires. The score of the Genta group was significantly lower at day 56 compared to the CTRL group (p = 0.0145) (Fig. 5A).
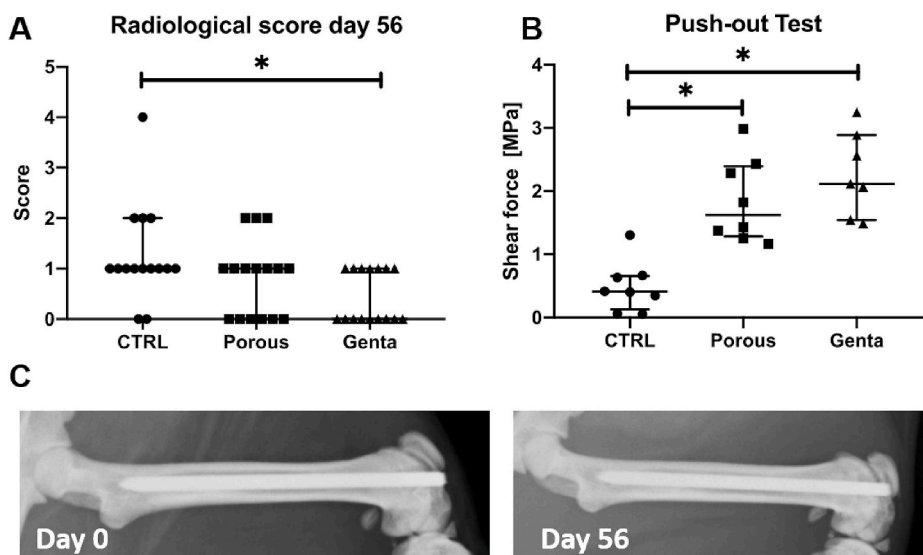

Fig. 5. Radiological and biomechanical analysis of the osteointegration after 56 days. A) The femora with the gentamicin K-wire showed a significantly lower score compared to CTRL (p = 0.0145). The maximum score possible is 15 points, which shows impaired osteointegration. B) The force needed to push the wire out of the femur was significantly higher in the Porous and Genta groups compared to CTRL (CTRL to Porous: p = 0.0153, CTRL to Genta: p = 0.0007). C) Representative x-ray on day 0 and day 56 from the same animal of the Porous group.

One K-wire of the Genta group was accidentally loosened during preparation and was therefore not measured. The maximum push-out shear force was significantly higher ($p \leq 0.0153$) in the Porous and Genta groups compared to the CTRL group. There was no statistical difference between the modified groups (Fig. 5B).

3.2.2.2. Histology and histomorphomeric analysis.
In the van Kossa/Safranin orange stain, the mineralized bone surrounding the K-wires was stained black, the cartilage was intense red, and the connective tissue was a lighter red.

One sample of the Porous group had partially abraded condyles and was excluded from the analysis of the fibrous tissue. Due to the intact diaphyseal ROI, the bone-implant contact could still be measured. There was significantly ($p = 0.0012$) more fibrous tissue formation in the CTRL group compared to the Porous group. The difference between the CTRL and Genta groups was not significant (Fig. 6A).

The CTRL group showed significantly less ($p = 0.0032$) bone-implant contact (BIC) compared to the Porous group and the Genta group (Fig. 6B). Newly formed bone filled the pores of the modified K-wires, resulting in increased direct contact (Fig. 6D).

3.3. Anti-infective properties

3.3.1. Release and antimicrobial activity
The release experiments revealed a burst release of 96% of the gentamicin within the first 30 min and a complete release after 1 h (Fig. 7A). The largest zones of inhibition (ZoI) occurred from the 30-min

elution samples and the size decreased over time (Fig. 7B and C). Wires taken at the end of the release experiments also induced an inhibition of *S. aureus* growth (Fig. 7D). This might be explained by the fluid/PBS that was still in the pores of the wire. No ZoI was seen when CTRL or Porous wires were placed on *S. aureus* coated agar plates.

3.3.2. Infection prophylaxis
The animals tolerated the surgery well but some showed intermittent, mild lameness (weight shifting while still bearing weight on all legs) in the first days after surgery. Therefore, a second dose of buprenorphine was administered subcutaneously in those animals for which pain elimination with tramadol alone did not appear to be sufficient. One animal of the Infection group died under anesthesia and one animal of the Genta group had to be euthanized due to a misplaced implant. Neither rats were replaced. The animals with *S. aureus* inoculation showed a weight loss 7 days after the operation (Table 1) with a significant reduction compared to CTRL in the Infection and Porous group on day 7, and the Porous group also on day 28. Six animals partially opened the sutures in the first days after the operation, resulting in partially secondary wound healing.

Animals were sacrificed after 28 days and the wires were explanted for microbiological analysis. The manual explantation of the Infection group K-wires was effortless as the infection had induced loosening. In contrast, 6 of the 8 K-wires of the Porous group and 5 of the 7 K-wires of the Genta group could only be explanted after carefully breaking the bony connections between the implant and the bone. One femur of the Genta group broke partially (condyles), but histological analysis was
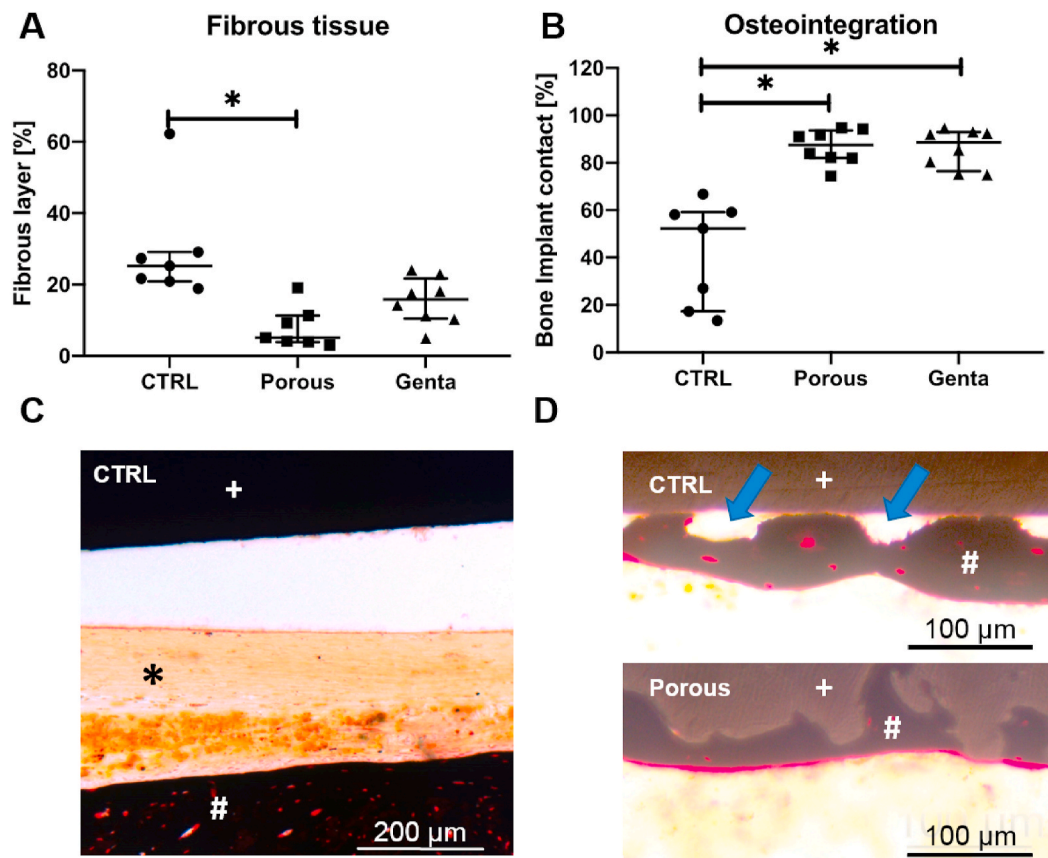

Fig. 6. Histological analysis of the osteointegration after 56 days. A) Significantly more connective tissue surrounded the K-wires of the CTRL group ($p = 0.0012$). B) The bone-implant contact was significantly higher in the Porous and Genta groups compared to CTRL ($p = 0.0032$). C) Example of connective tissue (black asterisk) between the CTRL wire (white plus sign) and the newly formed bone (white hash). D) High magnifications showing the growth of bone to the CTRL surface and the direct ingrowth of bone into the porous surface. Blue arrows: areas with no contact; white hash: newly formed bone; white plus sign: K-wire surface (upper picture: smooth control, lower picture: porous).
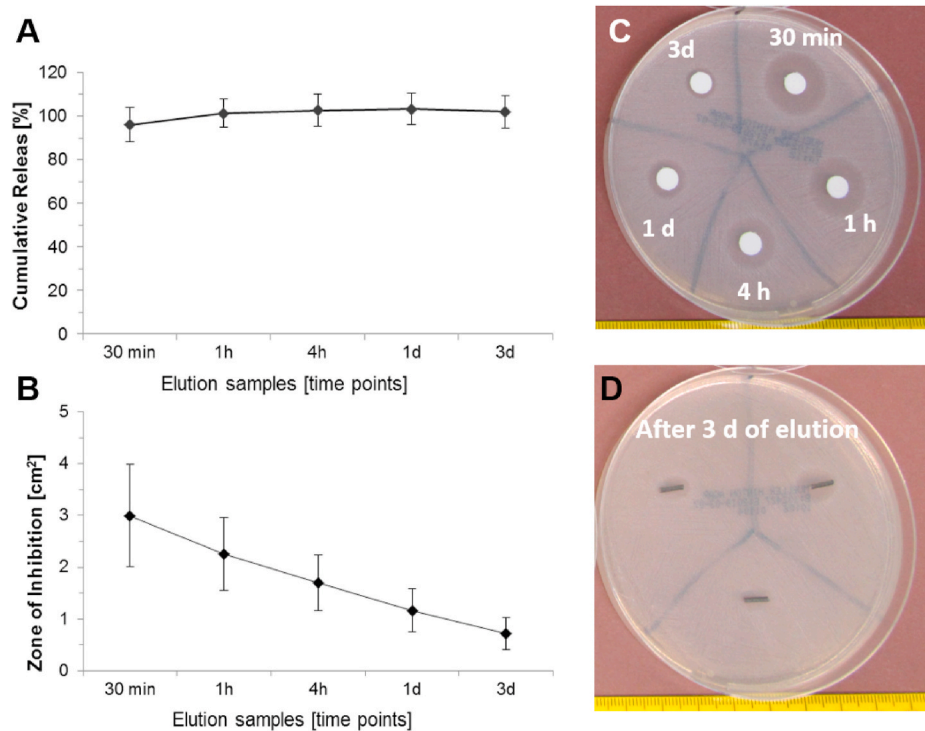
Fig. 7. Release and inhibition kinetics. A) Calculation of the cumulative gentamicin release showed a fast release within the first 30 min, followed by a slow and complete release within 1 h. B) Calculation of ZoI: the largest inhibition occurred with the 30 min eluate samples and decreased over the further time points. C) Exemplary ZoI from the eluate samples and D) from the Genta wires after 3 days of elution. ZoIs were clearly visible. n = 6 samples were used.

Table 1
Weight difference compared to the day of operation.

	CTRL	Infection	Porous	Genta
Δ Day 7	1.5%	−7%	−8%	−3%
	(0, 2)	(−11, −6)[a]	(−10.8, −5.3)[a]	(- 5, −2)
Δ Day 28	5.5%	−1%	−3%	1%
	(1.3, 7)	(−4, 3)	(−5, −0.3)[a]	(−2, 4)

[a] Day 7: CTRL-Infection p = 0.0002, CTRL-Porous p = 0.0003; Day 28: CTRL-Porous: p = 0.0027.

still possible.

Bacterial contamination of the implant was evident in 6 of the 7 animals from the Infection group, as demonstrated by roll-over cultures and the counting of CFUs after sonication (Fig. 8A, D). One animal without microbiological evidence of infection did not show signs of infection in the radiological pictures or bacterial findings and paraffin sections. All Porous wires were contaminated with *S. aureus* (Fig. 8B, D), whereas no bacterial growth was detected for the Genta (Fig. 8C and D) and CTRL wires (no *S. aureus*). A Gram staining was performed to further characterize the bacteria as *S. aureus* (Fig. 8E).

3.3.2.1. Osteomyelitis evaluation. The radiological analysis of the femora revealed clear signs of bone destruction in all animals of the Infection group (Fig. 9 A), milder signs in the Porous group, and no indication of osteomyelitis in the Genta group. Osteolysis and periosteal reactions were the most common changes to varying degrees: All femora of the Infection group showed severe to moderate changes, while in the Porous group mild changes of the cortical bone (2 of 8 animals) or small periosteal reactions (3 of 8 animals) were common. The radiological score showed significant differences between the Infection and the CTRL and Genta groups as well as the Porous and Genta groups (Fig. 9 B). The Infection group also had the highest scores for acute and chronic HOES, with significant differences to the CTRL and Genta groups (Fig. 9C, D). The score values for the Porous group were between the Infection

and the Genta groups, without significant differences to either of the groups.

3.3.2.2. Histological evaluation. The histological analysis confirmed the radiological pictures: The femora of the Infection group showed clear signs of osteomyelitis with an accumulation of neutrophils and lymphocytes as well as the formation of fibrosis and necrosis (Fig. 10A–C). The destruction of the bone was seen in the distal metaphysis and throughout the diaphysis. In total, 5 of the 7 femora of the Infection group and one femur of the Porous group showed severe changes. The other two femora of the Infection group had multiple small abscesses and granulomas. The changes of the femora of the CTRL and Genta groups (Fig. 10 G) were mostly minor fibrosis indicative of a foreign body reaction due to the implanted wire.

4. Discussion

The use of porous surfaces to promote osteointegration is state of the art, especially in the upper area of a hip prostheses stem [26]. In addition to the integration of porosity in the implant design from the start (casting or additive manufacturing), various post-processing technologies such as drilling, turning and milling are available to produce relatively rough surfaces. For a more rapid bone integration, fine (porous) structures are required and technologies like (plasma) anodization, grit- or sand-blasting, acid etching, laser structuring or coating technologies such as physical or chemical vacuum deposition, plasma-spraying or electrochemical deposition are used [27]. To reduce the infection risk, local antibiotic loading of the implants should be possible in a fast and easy manner. Clinical applicability was the main objective in the development of the presented porous surface to deliver a sterile implant that can be reproducibly loaded with pre-defined antibiotics (from the hospital pharmacy) directly into the operating theater and according to the results of an individually performed antibiotic sensitivity testing. The validated loading procedure, i.e. simply immersing the implant into
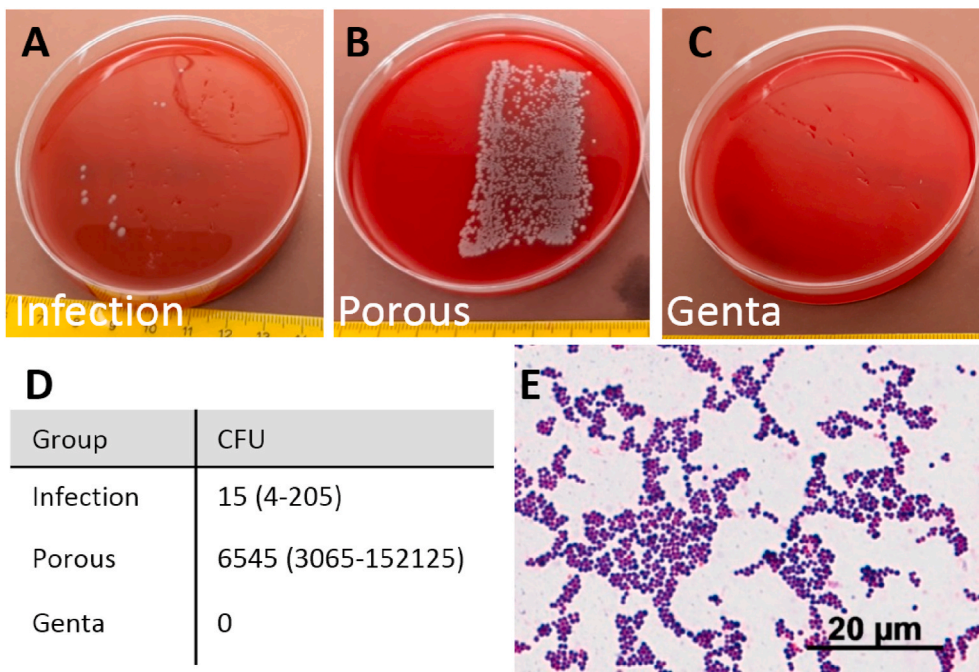
Fig. 8. Microbiological results of K-wires after explantation at day 28. A-C) Roll-over cultures from representative K-wires of the groups with *S. aureus* inoculation. (A) Few CFUs were detectable in the Infection group (smooth K-wire), (B) there was a high amount of CFUs in the Porous group, and (C) no CFUs grew from the gentamicin-loaded K-wires. D) The number of CFUs after sonication of the wires, median (25–75 percentile, n = 7–8 per group). E) Gram staining of the cells as a further identification of *S. aureus*.
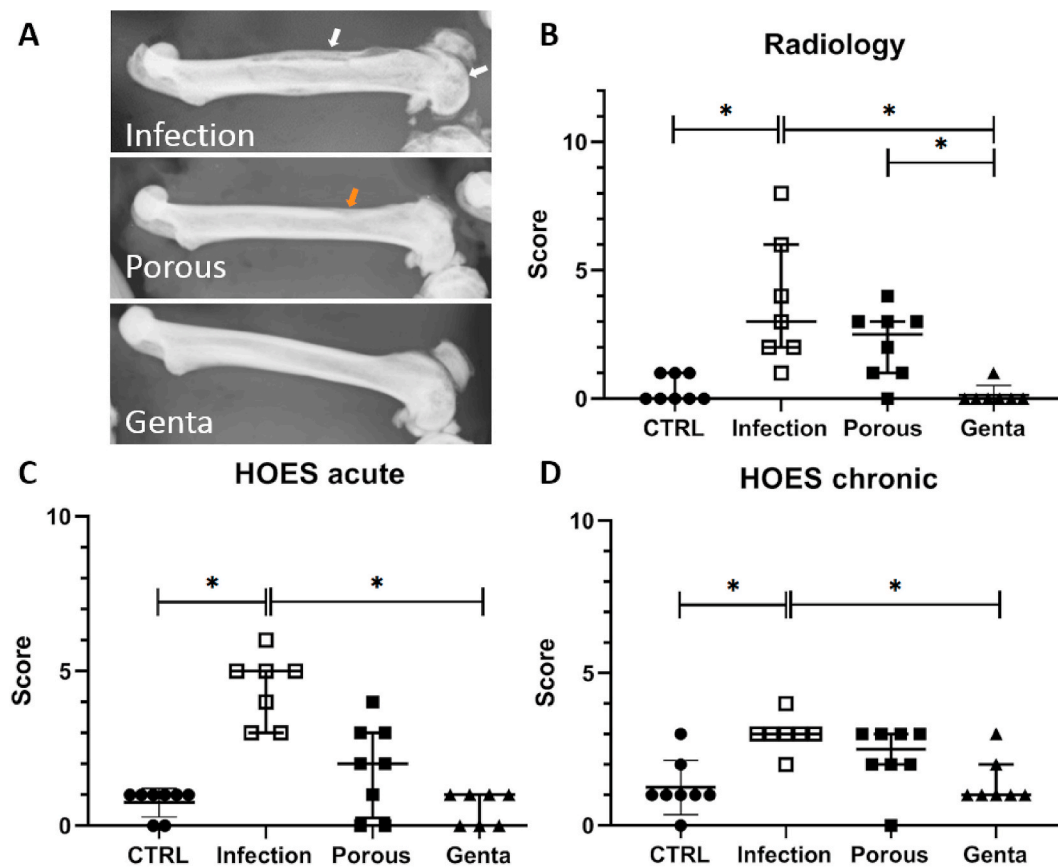
Group	CFU
Infection	15 (4-205)
Porous	6545 (3065-152125)
Genta	0

Fig. 9. Radiological and histological scoring at day 28. A) The femur of the Infection group showed clear signs of bony alterations and destructions in the condyle and the diaphyseal region, such as cortical thickening and new bone formation (white arrows). Small changes in the diaphyseal bone (red arrow) and the condyle were visible in the femur treated with the porous wire. The femur with the gentamicin-loaded wire was intact. B) Results of the radiologic scoring: The femora of the Infection group had significantly higher scores compared to the CTRL and Genta groups (p = 0.0077 and p = 0.0019). The difference between the Porous group and Genta group was also significant (p = 0.0314). C&D) The calculation of the acute and chronic HOES [25] showed the highest results for the Infection group and the lowest for the non-infected CTRL group (n = 7–8 per group). Significantly higher score values were detected for the Infection group compared to CTRL (acute p = 0.0024, chronic p = 0.0086). The HOES score for the Genta group was significantly lower compared to the Infection group (acute p = 0.0009, chronic p = 0.0286).
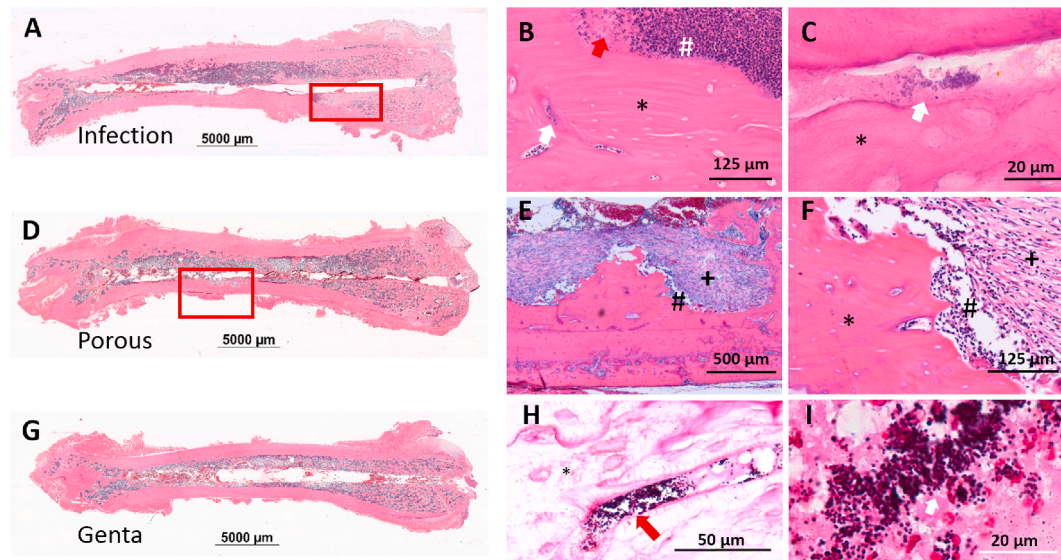
Fig. 10. Histological examples of the femora from the infection study. HE stained sections of A) the Infection group with a necrotic area (red rectangle); the former borders of the K-wire are clearly visible. D) The Porous group with a necrotic-fibrotic area of the mid-diaphysis (red rectangle). G) The Genta group without alteration to the bony structure. B) Higher magnification of the area marked by the red rectangle in A; white arrow: bacteria in necrotic bone; red arrow: necrotic debris; black asterisk: necrotic bone (empty osteocyte lacunae); white number sign: accumulation of neutrophilic granulocytes. C) Higher magnification of B; white arrow: bacteria; black asterisk: necrotic bone. E) Higher magnification of the area marked by red rectangle in D; black asterisk: necrotic bone; black number sign: accumulation of neutrophilic granulocytes; black plus: fibrosis. F) Higher magnification of E, same meaning of symbols as in E. H) Infection group: Gram-positive cocci in bone (red arrow) and necrotic bone (black asterisk). I) Gram-positive bacteria located in the vascular channels of necrotic bone and the necrotic debris of soft tissue and bone.

an antibiotic solution during the operation, has advantages compared to the dropwise application of the solution [28] or coatings [29–31]. Even if clinical acceptance is achieved, the hurdles for translation are development costs and, in particular, regulatory approval under applicable legal regulations [32]. These factors led us to **select laser technology**, which is environmentally friendly, has a large structuring scale (micro to nano structures), needs no auxiliary materials, is reproducible, and can be automated to structure complex products. Laser structuring is applicable to already regulatory cleared products and does not change the main intended use of the implant. The added antibiotic must be taken into account for translation from a regulatory point of view, but it does not represent a knock-out criterion, especially since approved devices for local gentamicin release can be used as a reference [33]. However, the area of surface structuring of the implant must carefully be considered regarding the possible mechanical impact of the surface finish. An increased fatigue failure due crack initiation by surface modifications is expected compared to polished, smooth surfaces [34].

The mechanical properties of the coating were characterized by different methods. The porous surface revealed a lap shear strength of 26 MPa and thus exceeded the requirements of ISO 13779–2:2018–12, which demand a bonding strength >15 MPa for thermally sprayed coatings of hydroxyapatite. In the pull-off test, the cohesion failed between the adhesive and the dolly at 7 MPa, but not between the porous structure and the implant. Higher forces might be possible with another pretreatment of the test dollies, as performed by Zimmermann et al. [35]. In general, the findings are in line with Parcharoen [36], who reported that the bonding strength of HA depends on the substrate, especially for porous substrates, and on the manufacturing parameters [37]. The bending modulus of 98 GPa for CTRL is close to the reported value of 110 GPa for solid titanium implants [38]. The reduced bending modulus of the Porous surface was expected due to the presence of multiple "notches" [17] and has to be considered in the implant design for load-bearing implants [39]. The application of an impact force on the porous surface resulted only in a surface scratch without coating loss or peeling, as reported by Duan et al. for HA coatings [40]. Further surface characteristics were determined by the wettability (contact angle)

measurements of the implant. The contact angle of 71° (advancing measurement) for the anodized K-wire (CTRL) was in line with the expectation for oxidized titanium surfaces, ranging from 69° to 85° [41]. The measured receding contact angle was smaller than the advancing contact angle, as described by Jennissen [42]. The modified porous K-wire, coated with titanium oxide after laser structuring, was hydrophilic with a contact angle of 9°. Compared to anodized hydrophobic titanium surfaces, a hydrophilic surface (such as the porous surface investigated here) can positively influence the osteogenic response, as described previously [43].

The combination of *in vitro* and *in vivo* studies proved the safety and efficacy of the active surface modification for the titanium implant presented here. Neither the porous silver-containing surface structuring nor the loading with gentamicin affected the vitality and differentiation of primary osteoblast-like cells. More importantly, both implant modifications showed an enhanced **osteointegration** in the rat femur model. The push-out force was significantly higher with the modified surfaces and the histological analysis revealed significantly more bone-implant contact. Implant modifications to prevent implant-associated infections have been extensively investigated (for a review see Refs. [44, 45]). The modifications include, for example, the use of coatings with antibacterial properties due to the coating material itself [46,47], with polymers for local drug release [30,48], the "grafting" of the surface through the use of anchorage molecules [49,50], and the structuring of the surface with and without post coatings [51,52].

For immediate antibacterial effectivity, the amphora-shaped pores of this surface can be loaded with a drug-containing solution that is completely released after 1 h, as shown for gentamicin. This immediate release will prevent bacterial adhesion that already occurs directly after implantation resulting in biofilm formation already after 1 h as shown for different orthopedic implant materials [53]. The embedded metallic silver particles could result in long-term protection due to the very slow release [54]. A detailed characterization of the structured surface revealed amphora-shaped pores that can be loaded with gentamicin and killed bacterial in direct contact while not affecting osteoblast adhesion and vitality [17,18]. This shape is due to the bottleneck, which is

optimal for drug loading and is assumed to improve the anchorage of newly formed bone. Human osteoblast like cells (MG-63) adhered to the porous surface and revealed a similar viability compared to smooth titanium over a period of 3 days. The here presented *in vitro* cytocompatibility testing and *in vivo* biocompatibility and osteointegration analyses proved this assumption and found no negative effect of the surface and the released gentamicin on osteoblast vitality or osteogenic differentiation. Only the alkaline phosphatase activity was reduced due to the gentamicin release. However, neither the cell vitality nor the mineralization (Alizarin red stain) was affected. It was previously shown that gentamicin reduced the alkaline phosphates activity at concentrations that have no effect on cell vitality [55,56]. The authors concluded that this might impair bone repair *in vivo*. Based on our *in vitro* results, gentamicin had only a negative effect on alkaline phosphatase after 21 days but not after 3 days. Interestingly, a recently published study found a transient negative effect of the 10x clinical concentration of gentamicin on cell proliferation but not on metabolic activity or mineralization [57]. The reduction of alkaline phosphatase was 20%, which might be within a tolerable range and without effect in an *in vivo* situation: The osteointegration was significantly enhanced by the surface modification, as determined by mechanical and histological analyses, and the local gentamicin release had no negative effect.

Yuan et al. recently reported on a titanium modification that showed good biocompatibility, osteointegration, and anti-infective properties [58]. The modification was based on a molybdenum disulfide/polydopamine-arginine-glycine-aspartic acid coating and the anti-infective effect was induced by near-infrared irradiation resulting in oxidative stress. The authors propose that an advantage of their treatment is the avoidance of a pharmaceutical approach, while the drawback is the more complicated production of the surface. It needs to be proven whether the near-infrared irradiation of the implanted material is transferable to the human situation and larger implants. Local hyperthermia (about 51 °C, rabbit model) can lead to reluctance.

In addition, the **anti-infective properties** of the porous titanium surface with silver nanoparticles and the possibility of an additional antibiotic drug loading were investigated. The local application of gentamicin reliably prevented the adherence of bacteria to the implant and the development of osteomyelitis in the femora, as shown by microbiological, radiographical, and histological analysis. In contrast, the Infection group showed clear histopathological signs, such as sequester formation, surrounded by inflammatory cells and fibrous tissue with microcolonies of bacteria adherent to the bone, which fits the picture of osteomyelitis [59]. The osteointegration in all groups with the modified surface was enhanced, resulting in a difficult K-wire explantation. This supports the findings from the biocompatibility study, in which a higher osteointegration was measured biomechanically and histologically. Interestingly, despite the good osteointegration in the Porous group, the animals showed a significant weight reduction at days 7 and 28 as an indicator for an infection [60]. Sonification of the Porous implants after explantation at day 28 revealed a high bacterial colonization, which might be explained by the rougher and porous surface that increases bacterial adhesion [15]. The bacteria were also found histologically in 6 of the 8 femora from that group. Nevertheless, the histological score of the Porous group revealed less severe changes in comparison to the Infection group. The long-term silver nanoparticle release may have prevented the progress of the osteomyelitis as the antibacterial characteristics of silver are well known [61–63]. Our previous study demonstrated a silver release *in vitro* and detected 14% release within the first day and 16% after 28 days [18]. Using a silver-silicon oxide layer on implants, Khalilpour et al. found an *in vivo* decrease in the silver from the initial 1.5 µg/cm^2 to 0.4 µg/cm^2 at 28 days after intramuscular implantation in rabbits [64]. A limitation of this study is the missing quantification of silver and gentamicin release *in vivo*. A synergistic effect of systemic antibiotic application and local silver nanoparticles on osteomyelitis prophylaxis was described previously [65]. Xu et al. hypothesize that the synergistic effect might be due

to, e.g., the destruction of the bacterial cell walls and/or attacking the 30S ribosomal subunit, which is the target of gentamicin [65]. As a limitation of the present study, it should be mentioned that no porous structure without additional silver nanoparticles was examined. Therefore, the possible effect of gentamicin with and without silver cannot be determined. However other promising studies with local silver release have been published, such as the recent work showing the release of silver ions from a laser-melted porous titanium surface over at least 28 days and the killing of methicillin-resistant *S. aureus* [66]. Free silver particles can also have a cytotoxic effect based on particle size and concentration [67], especially if bare metal silver is used as a coating. The silver used in the study described here is in the form of particles completely embedded in a layer and the cells or tissue only come into contact with silver ions released from this layer, meaning there is no direct cell-metallic silver contact. Therefore, it is possible that the mode of action is similar to silver nanoparticles embedded in titanium by plasma immersion ion implantation [68]. Silver nanoparticles embedded in titanium induced the production of reactive oxygen by electron transfer, which is responsible for the antimicrobial effect. The cyto- and biocompatibility analysis of the present study showed no negative effect of the structured surface with the deposited silver, but rather a better osteointegration *in vivo*. This is in accordance with a recently published study using the same deposition technique [69]. Whether the porous structure might perform better without silver was, however, not investigated in the present study. The released gentamicin had also no negative effect in the present study. Depending on the dosage, gentamicin can affect bone regeneration, as shown in previous studies. Fracture healing in a rat model was not impaired through the use of a gentamicin-coated nail [70]. The amount of gentamicin, approximately 102 µg gentamicin base/cm^2 (170 µg gentamicin sulfate/cm^2), was approximately four times lower than in the present study. A gentamicin-enriched graft, however, impaired the regeneration of a bony defect in a sheep model (total gentamicin dosage: 10 mg), although the *in vitro* data revealed no significant impairment of the osteoblasts [71]. The gentamicin loading used in the present study is within the middle range of previously published loadings, ranging from approximately 100 µg/cm^2 to 850 µg/cm^2 [28,72–74].

The **laser structuring** of metallic surfaces has previously been used to produce antibacterial surfaces. Doll et al. reported a slippery liquid-infused porous surface (SLIPS) produced by ultrashort pulsed laser ablation, which inhibited the adhesion of bacteria and fibroblasts [75]. They produced titanium surfaces with spikes, grooves or ripples and spin-loaded them with perfluoropolyether lubricants of different viscosities. The best antibiofilm results were obtained with the spiked structures, which also reduced fibroblast growth. A surface modification that inhibits the adhesion of endogenous cells is not favorable for implants that should integrate into the bone, such as prostheses, but might be useful for short-term implants, such as intramedullary nails. The use of spiked surfaces in a preclinical infection model, however, had no effect on the infection of the tibia, although there were antibacterial effects *in vitro* [76]. Surprisingly, it was more difficult to remove the spiked implant from the infected bone compared to the pure titanium implant. The radiological scores, histological analysis, and bacterial contamination, however, showed more bone destruction, fibrosis, and bacteria in the laser-structured group, which indicates poor osteointegration. Several other studies report the structuring and loading of titanium surfaces. The disadvantage of previously published loading methods for structured titanium surfaces are further preparations or chemicals needed and several loading and drying steps [29,77–79], while the presented amphora-shaped pores are loaded by their hydrophilic surface conditions and capillary forces without the need of further steps.

Two aspects are important for the successful **clinical translation** of new surface modifications: the manufacturing and the performance. To fulfill the requirements of medical device producers and regulatory authorities, the manufacturing process should be easy, reproducible,

validated, up-scalable, and applicable to already established implants. If antibiotics are used in combination with the surface modification, the surgeon should have the freedom to choose the antibacterial drug based on the clinical need. For example, for permanent implants, the modifications must kill the bacteria but should not harm the endogenous cells or inhibit osteointegration [80]. The **advantage** of the presented surface modification is the easy application to already approved metallic implants. The laser structuring results in minor metallographic changes of the titanium in that the microcrystalline structure is changed to a martensite structure within a depth of app. 66 μm, as demonstrated previously [17]. The loading with the drug of need is easy, reproducible, and can be done during the surgical procedure. However, further studies under regulatory compliant conditions, which also include biomechanical analysis, long term release *in vitro* and *in vivo* as well as antimicrobial studies, pharmacokinetic, preferably with the final implant material or, even better with the implant system, are required for a transfer from bench to bedside.

5. Conclusion

In conclusion, the amphora-shaped pores on titanium implants with or without gentamicin loading revealed good cyto- and biocompatibility and the gentamicin loading effectively prevented infection. The vitality and differentiation of primary human osteoblast-like cells were not affected, while osteointegration was enhanced. Antimicrobial effectivity by the local gentamicin release was shown *in vitro* and in a rat model. This surface modification can be applied to implants without the alteration of the metal properties and without further equipment or post-coating and might, therefore, be a promising option. Against the background of the data presented, this novel coating could shift the "race for the surface", as first mentioned by Anthony Gristina [7], in favor of the body's own cells, thus giving patients a head start in the fight against implant-associated infections.

Data availability

The data required to reproduce these findings are available upon request to the corresponding authors.

CRediT authorship contribution statement

Viviane Ständert: Investigation, Methodology, Validation, Visualization, Writing - review & editing. **Kai Borcherding:** Conceptualization, Data curation, Funding acquisition, Project administration, Investigation, Methodology, Resources, Supervision, Validation, Visualization, Writing - original draft. **Nicole Bormann:** Investigation, Validation, Visualization, Writing - review & editing. **Gerhard Schmidmaier:** Conceptualization, Writing - review & editing. **Ingo Grunwald:** Conceptualization, Formal analysis, Funding acquisition, Project administration, Resources, Writing - review & editing. **Britt Wildemann:** Conceptualization, Formal analysis, Funding acquisition, Project administration, Resources, Supervision, Visualization, Writing - original draft.

Declaration of competing interest

The authors declare that they have no known competing financial interests or personal relationships that could have appeared to influence the work reported in this paper.

References

[1] M. Sloan, A. Premkumar, N.P. Sheth, Projected volume of primary total joint arthroplasty in the U.S., 2014 to 2030, JBJS 100 (17) (2018) 1455–1460.

[2] E. Garcia-Rey, R. Carbonell-Escobar, J. Cordero-Ampuero, E. Garcia-Cimbrelo, Outcome of a hemispherical porous-coated acetabular component with a proximally hydroxyapatite-coated anatomical femoral component: an update at 23 to 26 years' follow-up, Bone Joint Lett. J 101-b (4) (2019) 378–385.

[3] S.M. Kurtz, E.C. Lau, M.-S. Son, E.T. Chang, W. Zimmerli, J. Parvizi, Are we winning or losing the battle with periprosthetic joint infection: trends in periprosthetic joint infection and mortality risk for the medicare population, J. Arthroplasty 33 (10) (2018) 3238–3245.

[4] H.M. Wolford, K.M. Hatfield, P. Paul, S.H. Yi, R.B. Slayton, The projected burden of complex surgical site infections following hip and knee arthroplasties in adults in the United States, 2020 through 2030, Infect. Control Hosp. Epidemiol. 39 (10) (2018) 1189–1195.

[5] E. Seebach, K.F. Kubatzky, Chronic implant-related bone infections-can immune modulation be a therapeutic strategy? Front. Immunol. 10 (2019) 1–21.

[6] E. Mariani, G. Lisignoli, R.M. Borzi, L. Pulsatelli, Biomaterials: foreign bodies or tuners for the immune response? Int. J. Mol. Sci. 20 (3) (2019) 1–42.

[7] A.G. Gristina, Biomaterial-centered infection: microbial adhesion versus tissue integration, Science 237 (4822) (1987) 1588–1595.

[8] D.J. Davidson, D. Spratt, A.D. Liddle, Implant materials and prosthetic joint infection: the battle with the biofilm, EFORT Open Rev. 4 (11) (2019) 633–639.

[9] L. Damiati, M.G. Eales, A.H. Nobbs, B. Su, P.M. Tsimbouri, M. Salmeron-Sanchez, M.J. Dalby, Impact of surface topography and coating on osteogenesis and bacterial attachment on titanium implants, J. Tissue Eng. 9 (2018) 1–16.

[10] S.C. Sartoretto, A.T.N.N. Alves, L. Zarranz, M.Z. Jorge, J.M. Granjeiro, M. D. Calasans-Maia, Hydrophilic surface of Ti6Al4V-ELI alloy improves the early bone apposition of sheep tibia, Clin. Oral Implants Res. 28 (8) (2017) 893–901.

[11] I. De Tullio, M. Berardini, D. Di Iorio, F. Perfetti, G. Perfetti, Comparative evaluation among laser-treated, machined, and sandblasted/acid-etched implant surfaces: an in vivo histologic analysis on sheep, Int. J. Implant Dent. 6 (1) (2020) 1–8.

[12] K. Pałka, R. Pokrowiecki, Porous titanium implants: a review, Adv. Eng. Mater. 20 (5) (2018) 1–18.

[13] A. Palmquist, L. Emanuelsson, R. Brånemark, P. Thomsen, Biomechanical, histological and ultrastructural analyses of laser micro- and nano-structured titanium implant after 6 months in rabbit, J. Biomed. Mater. Res. B Appl. Biomater. 97B (2) (2011) 289–298.

[14] J. Li, X. Cui, G.J. Hooper, K.S. Lim, T.B.F. Woodfield, Rational design, bio-functionalization and biological performance of hybrid additive manufactured titanium implants for orthopaedic applications: a review, J. Mech. Behav. Biomed. Mater. 105 (2020) 1–18.

[15] W. Orapiriyakul, P.S. Young, L. Damiati, P.M. Tsimbouri, Antibacterial surface modification of titanium implants in orthopaedics, J. Tissue Eng. 9 (2018) 1–16.

[16] S. Qin, K. Xu, B. Nie, F. Ji, H. Zhang, Approaches based on passive and active antibacterial coating on titanium to achieve antibacterial activity, J. Biomed. Mater. Res. 106 (9) (2018) 2531–2539.

[17] K. Borcherding, D. Marx, L. Gätjen, U. Specht, D. Salz, K. Thiel, B. Wildemann, I. Grunwald, Impact of laser structuring on medical-grade titanium: surface characterization and in vitro evaluation of osteoblast attachment, Materials 13 (8) (2020) 1–12.

[18] K. Borcherding, D. Marx, L. Gatjen, N. Bormann, B. Wildemann, U. Specht, D. Salz, K. Thiel, I. Grunwald, Burst release of antibiotics combined with long-term release of silver targeting implant-associated infections: design, characterization and in vitro evaluation of novel implant hybrid surface, Materials 12 (23) (2019) 1–13.

[19] Huntsman-Advanced-Materials, Araldite® 2011. Two Component Epoxy Adhesive, Technical data sheet, 2014.

[20] S. Lüers, C. Seitz, M. Laub, H.P. Jennissen, Contact angle measurement on dental implants, Biomed. Eng./Biomed. Tech. 59 (2014) 91–95.

[21] D.A. Back, S. Pauly, L. Rommel, N.P. Haas, G. Schmidmaier, B. Wildemann, S. H. Greiner, Effect of local zoledronate on implant osseointegration in a rat model, BMC Muscoskel. Disord. 13 (2012) 1–9.

[22] W.S. Rasband, U.S. ImageJ, National Institutes of Health, Bethesda, Maryland, USA, 1997. https://imagej.nih.gov/ij/.

[23] N. Bormann, P. Schwabe, M.D. Smith, B. Wildemann, Analysis of parameters influencing the release of antibiotics mixed with bone grafting material using a reliable mixing procedure, Bone 59 (2014) 162–172.

[24] S. Das, K. Dholam, S. Gurav, K. Bendale, A. Ingle, B. Mohanty, P. Chaudhari, J. R. Bellare, Accentuated osseointegration in osteogenic nanofibrous coated titanium implants, Sci. Rep.-Uk 9 (1) (2019) 17638.

[25] A. Tiemann, G.O. Hofmann, M.G. Krukemeyer, V. Krenn, S. Langwald, Histopathological Osteomyelitis Evaluation Score (HOES) - an innovative approach to histopathological diagnostics and scoring of osteomyelitis, GMS Interdiscipl. Plastic Reconstruct. Surg. DGPW 3 (2014) 1–12.

[26] T. McTighe, D. Brazil, J. Keggi, L. Keppler, E. Mcpherson, The adult hip: hip arthroplasty surgery, in: C.J. Della Valle, H.E. Rubash, J.J. Callaghan, J.C. Clohisy, P.E. Beaulé (Eds.), Short-stem Designs for Total Hip Arthroplasty: Neck Stabilized Femoral Components, Wolters Kluwer Philadelphia, 2016, pp. 823–849.

[27] Q. Wang, P. Zhou, S. Liu, S. Attarilar, R.L. Ma, Y. Zhong, L. Wang, Multi-scale surface treatments of titanium implants for rapid osseointegration: a review, Nanomaterials 10 (6) (2020).

[28] V. Alt, A. Bitschnau, J. Osterling, A. Sewing, C. Meyer, R. Kraus, S.A. Meissner, S. Wenisch, E. Domann, R. Schnettler, The effects of combined gentamicin-hydroxyapatite coating for cementless joint prostheses on the reduction of infection rates in a rabbit infection prophylaxis model, Biomaterials 27 (26) (2006) 4627–4634.

[29] M. Diefenbeck, C. Schrader, F. Gras, T. Muckley, J. Schmidt, S. Zankovych, J. Bossert, K.D. Jandt, A. Volpel, B.W. Sigusch, H. Schubert, S. Bischoff, W. Pfister, B. Edel, M. Faucon, U. Finger, Gentamicin coating of plasma chemical oxidized titanium alloy prevents implant-related osteomyelitis in rats, Biomaterials 101 (2016) 156–164.

[30] G. Schmidmaier, B. Wildemann, A. Stemberger, N.P. Haas, M. Raschke, Biodegradable poly(D,L-lactide) coating of implants for continuous release of growth factors, J. Biomed. Mater. Res. 58 (4) (2001) 449–455.

[31] T. Wang, Z. Weng, X. Liu, K.W.K. Yeung, H. Pan, S. Wu, Controlled release and biocompatibility of polymer/titania nanotube array system on titanium implants, Bioactive Mater. 2 (1) (2017) 44–50.

[32] H.J. Busscher, V. Alt, H.C. van der Mei, P.H. Fagette, W. Zimmerli, T.F. Moriarty, J. Parvizi, G. Schmidmaier, M.J. Raschke, T. Gehrke, R. Bayston, L.M. Baddour, L. C. Winterton, R.O. Darouiche, D.W. Grainger, A trans-atlantic perspective on stagnation in clinical translation of antimicrobial strategies for the control of biomaterial-implant-associated infection, ACS Biomater. Sci. Eng. 5 (2) (2019) 402–406.

[33] G. Schmidmaier, M. Kerstan, P. Schwabe, N. Sudkamp, M. Raschke, Clinical experiences in the use of a gentamicin-coated titanium nail in tibia fractures, Injury 48 (10) (2017) 2235–2241.

[34] M. Niinomi, 5 - fatigue failure of metallic biomaterials, in: M. Niinomi (Ed.), Metals for Biomedical Devices (second ed.), Woodhead Publishing2019, pp. 153-188.

[35] S. Zimmermann, U. Specht, L. Spieß, H. Romanus, S. Krischok, M. Himmerlich, J. Ihde, Improved adhesion at titanium surfaces via laser-induced surface oxidation and roughening, Mater. Sci. Eng., A 558 (2012) 755–760.

[36] Y. Parcharoen, P. Termsuksawad, S. Sirivisoot, Improved bonding strength of hydroxyapatite on titanium dioxide nanotube Arrays following alkaline pretreatment for orthopedic implants, J. Nanomater. 2016 (2016) 9143969.

[37] E. Mohseni, E. Zalnezhad, A.R. Bushroa, Comparative investigation on the adhesion of hydroxyapatite coating on Ti–6Al–4V implant: a review paper, Int. J. Adhesion Adhes. 48 (2014) 238–257.

[38] M. Takemoto, S. Fujibayashi, M. Neo, J. Suzuki, T. Kokubo, T. Nakamura, Mechanical properties and osteoconductivity of porous bioactive titanium, Biomaterials 26 (30) (2005) 6014–6023.

[39] J.C. Dick, C.A. Bourgeault, Notch sensitivity of titanium alloy, commercially pure titanium, and stainless steel spinal implants, Spine 26 (15) (2001) 1668–1672.

[40] Y. Duan, S. Zhu, F. Guo, J. Zhu, M. Li, J. Ma, Q. Zhu, The effect of adhesive strength of hydroxyapatite coating on the stability of hydroxyapatite-coated prostheses in vivo at the early stage of implantation, Arch. Med. Sci. 8 (2) (2012) 199–208.

[41] A.S. Zuruzi, Y.H. Yeo, A.J. Monkowski, C.S. Ding, N.C. MacDonald, Superhydrophilicity on microstructured titanium surfaces via a superficial titania layer with interconnected nanoscale pores, Nanotechnology 24 (24) (2013) 1–9.

[42] H.P. Jennissen, Hyperhydrophilic rough surfaces and imaginary contact angles, Mater. Werkst. 43 (8) (2012) 743–750.

[43] E.M. Lotz, R. Olivares-Navarrete, S. Berner, B.D. Boyan, Z. Schwartz, Osteogenic response of human MSCs and osteoblasts to hydrophilic and hydrophobic nanostructured titanium implant surfaces, J. Biomed. Mater. Res. 104 (12) (2016) 3137–3148.

[44] K. Vasilev, J. Cook, H.J. Griesser, Antibacterial surfaces for biomedical devices, Expet Rev. Med. Dev. 6 (5) (2009) 553–567.

[45] H. Chouirfa, H. Bouloussa, V. Migonney, C. Falentin-Daudre, Review of titanium surface modification techniques and coatings for antibacterial applications, Acta Biomater. 83 (2019) 37–54.

[46] E. Peeters, G. Hooyberghs, S. Robijns, A. De Weerdt, S. Kucharikova, H. Tournu, A. Braem, K. Ceh, G. Majdic, T. Spanic, E. Pogorevc, B. Claes, B. Dovgan, L. Girandon, F. Impellizzeri, M. Erdtmann, A. Krona, J. Vleugels, M. Frohlich, J. Garcia-Forgas, K. De Brucker, B.P.A. Cammue, K. Thevissen, P. Van Dijck, J. Vanderleyden, E. Van der Eycken, H.P. Steenackers, An antibiofilm coating of 5-aryl-2-aminoimidazole covalently attached to a titanium surface, J. Biomed. Mater. Res. B Appl. Biomater. 107 (6) (2019) 1908–1919.

[47] K. Vogel, N. Westphal, D. Salz, K. Thiel, L. Wittig, L.C. Ciacchi, I. Grunwald, Dental implants coated with a durable and antibacterial film, Surface Innov. 3 (1) (2015) 27–38.

[48] W. Boot, H.C. Vogely, C. Jiao, P.G. Nikkels, B. Pouran, M.H. van Rijen, M. B. Ekkelenkamp, G.M. Hansch, W.J. Dhert, D. Gawlitta, Prophylaxis of implant-related infections by local release of vancomycin from a hydrogel in rabbits, Eur. Cell. Mater. 39 (2020) 108–120.

[49] I.M. Shapiro, N.J. Hickok, J. Parvizi, S. Stewart, T.P. Schaer, Molecular engineering of an orthopaedic implant: from bench to bedside, Eur. Cell. Mater. 23 (2012) 362–370.

[50] G. Boix-Lemonche, J. Guillem-Marti, F. D'Este, J.M. Manero, B. Skerlavaj, Covalent grafting of titanium with a cathelicidin peptide produces an osteoblast compatible surface with antistaphylococcal activity, Colloids Surf. B Biointerfaces 185 (2020) 1–10.

[51] Y. Li, Y. Yang, R. Li, X. Tang, D. Guo, Y. Qing, Y. Qin, Enhanced antibacterial properties of orthopedic implants by titanium nanotube surface modification: a review of current techniques, Int. J. Nanomed. 14 (2019) 7217–7236.

[52] M. Khodaei, A. Valanezhad, I. Watanabe, Controlled gentamicin- strontium release as a dual action bone agent: combination of the porous titanium scaffold and biodegradable polymers, J. Alloys Compd. 720 (2017) 22–28.

[53] H. Koseki, A. Yonekura, T. Shida, I. Yoda, H. Horiuchi, Y. Morinaga, K. Yanagihara, H. Sakoda, M. Osaki, M. Tomita, Early staphylococcal biofilm formation on solid orthopaedic implant materials: in vitro study, PloS One 9 (10) (2014), e107588.

[54] P. Khalilpour, K. Lampe, M. Wagener, B. Stigler, C. Heiss, M.S. Ullrich, E. Domann, R. Schnettler, V. Alt, Ag/SiOxCy plasma polymer coating for antimicrobial protection of fracture fixation devices, J. Biomed. Mater. Res. B Appl. Biomater. 94B (1) (2010) 196–202.

[55] S. Isefuku, C.J. Joyner, A.H. Simpson, Gentamicin may have an adverse effect on osteogenesis, J. Orthop. Trauma 17 (3) (2003) 212–216.

[56] C.R. Rathbone, J.D. Cross, K.V. Brown, C.K. Murray, J.C. Wenke, Effect of various concentrations of antibiotics on osteogenic cell viability and activity, J. Orthop. Res. 29 (7) (2011) 1070–1074.

[57] A.M. Philp, S. Raja, A. Philp, M.P. Newton Ede, S.W. Jones, The effect of vancomycin and gentamicin antibiotics on human osteoblast proliferation, metabolic function, and bone mineralization, Spine 42 (3) (2017) 202–207.

[58] Z. Yuan, B. Tao, Y. He, J. Liu, C. Lin, X. Shen, Y. Ding, Y. Yu, C. Mu, P. Liu, K. Cai, Biocompatible MoS2/PDA-RGD coating on titanium implant with antibacterial property via intrinsic ROS-independent oxidative stress and NIR irradiation, Biomaterials 217 (2019) 119290.

[59] J.H. Calhoun, M.M. Manring, M. Shirtliff, Osteomyelitis of the long bones, Semin. Plast. Surg. 23 (2) (2009) 59–72.

[60] Y.H. An, Q.K. Kang, C.R. Arciola, Animal models of osteomyelitis, Int. J. Artif. Organs 29 (4) (2006) 407–420.

[61] D.J. Barillo, D.E. Marx, Silver in medicine: a brief history BC 335 to present, Burns 40 (Suppl 1) (2014) S3–8.

[62] Y. Qing, L. Cheng, R. Li, G. Liu, Y. Zhang, X. Tang, J. Wang, H. Liu, Y. Qin, Potential antibacterial mechanism of silver nanoparticles and the optimization of orthopedic implants by advanced modification technologies, Int. J. Nanomed. 13 (2018) 3311–3327.

[63] M.B. Sedelnikova, E.G. Komarova, Y.P. Sharkeev, A.V. Ugodchikova, T. V. Tolkacheva, J.V. Rau, E.E. Buyko, V.V. Ivanov, V.V. Sheikin, Modification of titanium surface via Ag-, Sr- and Si-containing micro-arc calcium phosphate coating, Bioactive Mater. 4 (2019) 224–235.

[64] P. Khalilpour, K. Lampe, M. Wagener, B. Stigler, C. Heiss, M.S. Ullrich, E. Domann, R. Schnettler, V. Alt, Ag/SiO(x)C(y) plasma polymer coating for antimicrobial protection of fracture fixation devices, J. Biomed. Mater. Res. B Appl. Biomater. 94 (1) (2010) 196–202.

[65] N. Xu, H. Cheng, J. Xu, F. Li, B. Gao, Z. Li, C. Gao, K. Huo, J. Fu, W. Xiong, Silver-loaded nanotubular structures enhanced bactericidal efficiency of antibiotics with synergistic effect in vitro and in vivo, Int. J. Nanomed. 12 (2017) 731–743.

[66] I.A.J. van Hengel, N.E. Putra, M.W.A.M. Tierolf, M. Minneboo, A.C. Fluit, L. E. Fratila-Apachitei, I. Apachitei, A.A. Zadpoor, Biofunctionalization of selective laser melted porous titanium using silver and zinc nanoparticles to prevent infections by antibiotic-resistant bacteria, Acta Biomater. 107 (2020) 325–337.

[67] C.E. Albers, W. Hofstetter, K.A. Siebenrock, R. Landmann, F.M. Klenke, In vitro cytotoxicity of silver nanoparticles on osteoblasts and osteoclasts at antibacterial concentrations, Nanotoxicology 7 (1) (2013) 30–36.

[68] G. Wang, W. Jin, A.M. Qasim, A. Gao, X. Peng, W. Li, H. Feng, P.K. Chu, Antibacterial effects of titanium embedded with silver nanoparticles based on electron-transfer-induced reactive oxygen species, Biomaterials 124 (2017) 25–34.

[69] A. Radtke, M. Grodzicka, M. Ehlert, T. Jedrzejewski, M. Wypij, P. Golinska, To be microbiocidal and not to Be cytotoxic at the same time..."-silver nanoparticles and their main role on the surface of titanium alloy implants, J. Clin. Med. 8 (3) (2019) 1–23.

[70] M. Fassbender, S. Minkwitz, Z. Kronbach, C. Strobel, A. Kadow-Romacker, G. Schmidmaier, B. Wildemann, Local gentamicin application does not interfere with bone healing in a rat model, Bone 55 (2) (2013) 298–304.

[71] E. Beuttel, N. Bormann, A.M. Pobloth, G.N. Duda, B. Wildemann, Impact of gentamicin-loaded bone graft on defect healing in a sheep model, Materials 12 (7) (2019) 1–9.

[72] S. Nast, M. Fassbender, N. Bormann, S. Beck, A. Montali, M. Lucke, G. Schmidmaier, B. Wildemann, In vivo quantification of gentamicin released from an implant coating, J. Biomater. Appl. 31 (1) (2016) 45–54.

[73] D. Neut, R.J. Dijkstra, J.I. Thompson, C. Kavanagh, H.C. van der Mei, H. J. Busscher, A biodegradable gentamicin-hydroxyapatite-coating for infection prophylaxis in cementless hip prostheses, Eur. Cell. Mater. 29 (2015) 42–55, discussion 55-6.

[74] K.Y. Gudz, E.S. Permyakova, A.T. Matveev, A.V. Bondarev, A.M. Manakhov, D. A. Sidorenko, S.Y. Filippovich, A.V. Brouchkov, D.V. Golberg, S.G. Ignatov, D. V. Shtansky, Pristine and antibiotic-loaded nanosheets/nanoneedles-based boron nitride films as a promising platform to suppress bacterial and fungal infections, ACS Appl. Mater. Interfaces 12 (38) (2020) 42485–42498.

[75] K. Doll, E. Fadeeva, J. Schaeske, T. Ehmke, A. Winkel, A. Heisterkamp, B. N. Chichkov, M. Stiesch, N.S. Stumpp, Development of laser-structured liquid-infused titanium with strong biofilm-repellent properties, ACS Appl. Mater. Interfaces 9 (11) (2017) 9359–9368.

[76] M.L. Schroder, N. Angrisani, E. Fadeeva, J. Hegermann, J. Reifenrath, Laser-structured spike surface shows great bone integrative properties despite infection in vivo, Mater. Sci. Eng. C Mater. Biol. Appl. 109 (2020) 1–11.

[77] K.C. Popat, M. Eltgroth, T.J. Latempa, C.A. Grimes, T.A. Desai, Decreased Staphylococcus epidermis adhesion and increased osteoblast functionality on antibiotic-loaded titania nanotubes, Biomaterials 28 (32) (2007) 4880–4888.

[78] S.W. Park, D. Lee, Y.S. Choi, H.B. Jeon, C.-H. Lee, J.-H. Moon, I.K. Kwon, Mesoporous TiO2 implants for loading high dosage of antibacterial agent, Appl. Surf. Sci. 303 (2014) 140–146.

[79] D. Liu, C. He, Z. Liu, W. Xu, Gentamicin coating of nanotubular anodized titanium implant reduces implant-related osteomyelitis and enhances bone biocompatibility in rabbits, Int. J. Nanomed. 12 (2017) 5461–5471.

[80] C. Mas-Moruno, B. Su, M.J. Dalby, Multifunctional coatings and nanotopographies: toward cell instructive and antibacterial implants, Adv. Healthc. Mater. 8 (1) (2019), e1801103.